Zhao, W., Sun, H., Wang, Y., Eastoe, J., Dong, S., & Hao, J. (2018). Self-Assembled Magnetic Viruslike Particles for Encapsulation and Delivery of Deoxyribonucleic Acid. *Langmuir*, *34*(24), 7171-7179. https://doi.org/10.1021/acs.langmuir.8b01445

Self-Assembled Magnetic Virus-Like Particles for Encapsulation and Delivery of DNA

Wenrong Zhao,[†] Hong Sun,[†] Yitong Wang,[†] Julian Eastoe,[‡] Shuli Dong[†] and Jingcheng Hao*,[†]

[†] Key Laboratory of Colloid and Interface Chemistry & Key Laboratory of Special Aggregated Materials (Shandong University), Ministry of Education, Jinan 250100, P. R. China. E-mail: jhao@sdu.edu.cn

[‡] School of Chemistry, University of Bristol, Cantock's Close, Bristol BS8 1TS, U K.

Developing nontoxic artificial carriers for stimuli-responsive capture, transport and delivery of biomolecules is of immense scientific interest. Herein, for the first time, we synthesize a double-tailed cationic surfactant, $(C_{16}H_{33})_2(CH_3)_2N^+[FeCl_3Br]^-$, which possesses magnetic properties (Mag-Surf). The time-dependent formation of virus-shaped hybrid mixed assemblies of polyoxometalates (POM) $\{Mo_{72}Fe_{30}\}$/Mag-Surf with hollow shell structures is followed. These structures serve well as robust high-surface-area shuttles which can be manipulated with applied magnetic fields. By using cationic Mag-Surfs the anionic POMs and DNA can be complexed in these ternary mixtures. These virus-shaped complexes act as nano-anchors and nano-motors which can be utilized for binding, anchoring and delivery of biomolecules, such as DNA. It is found they have a good absorption capacity for DNA and Myoglobin over 24 hours, after application of a magnetic field. The realization of magnetic virus-shaped $\{Mo_{72}Fe_{30}\}$/Mag-Surf spheres may open possibilities for designing other functional nanoparticles allowing effective control over the delivery/separation of biomolecules.

Keywords: *magnetic surfactant, polyoxometalates, virus-shaped sphere, dynamic interface, biomolecule delivery*

Introduction

Creating anchored carriers with exceptional binding affinity for easy transport of biomolecules is critical in biotechnology. Nano-spheres fabricated of transition-metal phosphate,[1] silica,[2] porphyrin,[3] polypeptide,[4] gold[5] and silver[6] have been used in many applications, especially in well-defined nano-structures such as nanocubes, colloidal eggs[7] and *Janus* particles.[8] Key areas of interest for researchers in nano-scale bio-materials are separation of DNA and protein, magnetic resonance imaging, and drug delivery.[9,10] In order to improve efficiency and flexibility of encapsulation of biomacromolecules and heavy metal ions, high-surface-area structures have been generated, such as macroporous polymer particles with interconnected chambers,[11] high-surface-area nanospheres with a fibrous morphology,[2] and dual pore mesoporous carbon@silica composite core-shell nanospheres.[9c,10] Other concepts and strategies, like molecular motors[12] and shuttle-mediated drug delivery,[13] have been recently explored. Various potential methods have been reported for controlled adsorption and separation of proteins using applied electric potential[14] or magnetic fields.[15] As a non-invasive approach, magnetic separation of proteins has achieved success using remote-controlled magnetic nanoparticles.[15] With these applications in mind, developing novel, efficient magnetic nanoparticles of controlled morphology is desirable.

Cationic magnetic surfactants (Mag-Surf)[16] have certain advantages over nanoparticles on account of their easy fabrication (one-step synthesis), excellent dispersibility and stability in solution, and their ability to complex with anionic

DNA.[17] Magnetic polyoxometalates (POMs) {$Mo_{72}Fe_{30}$} ($Mo_{72}^{VI}Fe_{30}^{III}O_{252}L_{102}\cdot xH_2O$, x = 180, L = H_2O, CH_3COO^-, $Mo_2O_{8.9}^{n-}$), are water-soluble inorganic paramagnetic molecules with diameters of ca. 2.5 nm,[18] which are negatively charged in solution, because water ligands attached to the Fe^{III} centers tend to partially deprotonate. Though possessing potential magnetism, seldom has anyone succeeded in directly using POMs for negatively-charged target molecules (such as DNA), because both POMs and DNA carry negative charges. One alternative strategy, which is employed here, is to introduce Mag-Surfs, bearing positively-charged head-groups into POM systems, to create the needed charge difference.

Surfactants have been used for the transportation and compaction of DNA,[17] and cationic surfactants can bind to the DNA backbone, reduce the repulsion between adjacent DNA phosphate groups and allow them to approach each other, i.e., *compaction* of DNA.[19,20] Mag-Surfs, on account of their special magnetic counter-anions such as $[FeCl_3Br]^{-}$[16] and propensity to aggregate,[21] have previously been applied to absorb and migrate biomolecules,[22] however, the relatively weak magnetism may limit the efficiency for transporting biomolecules. As molecular building blocks for functional nanoscale systems,[23,24] POMs also can be developed as nanostructured assemblies especially if associated with amphiphilic moieties. In this paper, a Mag-Surf with two long alkyl chains, $(C_{16}H_{33})_2(CH_3)_2N^+[FeCl_3Br]^-$, is synthesized and serves as the amphiphilic moiety, which is both paramagnetic and hydrophobic. {$Mo_{72}Fe_{30}$} is employed as the building block to form POM-based surfactant hybrid spheres. We hypothesized that both {$Mo_{72}Fe_{30}$} and

$(C_{16}H_{33})_2(CH_3)_2N^+[FeCl_3Br]^-$ are introduced into the multi-magnetic-component POM/surfactant hybrid spheres, they could be used as nanosized magnetic vehicles to separate, transport, and anchor biomolecules. In such a multi-magnetic-component system, the magnetism is also strengthened via the combination of $\{Mo_{72}Fe_{30}\}$ and $(C_{16}H_{33})_2(CH_3)_2N^+[FeCl_3Br]^-$.

In this work a double-tailed cationic Mag-Surf $(C_{16}H_{33})_2(CH_3)_2N^+[FeCl_3Br]^-$ (Figure S1, Supporting Information) has been synthesized to act a charge regulation in these ternary complexes. Virus-shaped hybrid assemblies (**Scheme 1**) of $\{Mo_{72}Fe_{30}\}$[25]/Mag-Surf with hollow shell structures were fabricated by a dynamic interfacial process. To the best of our knowledge, such high-specific-area virus-shaped spheres composed of many smaller spheres have not been reported before. The robustness of these virus-shaped self-assembled particles after dilution facilitates binding, anchoring and delivery of DNA. At high concentrations these virus-shaped spheres (84.8 $\mu mol \cdot L^{-1}$) with DNA (150 $\mu mol \cdot L^{-1}$), it was possible to achieve 95% DNA absorption capacity within 24 hrs. Even at very low concentration of the magnetic virus-shaped spheres (3.71 $\mu mol \cdot L^{-1}$), capture and transport of DNA at 68% was still possible (Scheme 1) by applying only a low strength magnetic field (0.3 T). In addition, this system allows DNA to be anchored reversibly on the virus-shaped spheres by regulating electrostatic interactions with added NaBr electrolyte. The unique features of this system include:

1) magnetism is enhanced owing to the combination of two magnetic components: $(C_{16}H_{33})_2(CH_3)_2N^+[FeCl_3Br]^-$ inorganic macroions, $\{Mo_{72}Fe_{30}\}$;

2) the specific surface area of the assemblies is increased by formation of virus-shaped particles composed of smaller subsidiary hollow shell spheres;

3) owing to the presence of positively-charged Mag-Surfs, POM and DNA, which are both anionic, can be incorporated in one complex;

4) the strong electrostatic interacts act as nano-anchors, and magnetic properties give rise to a nano-motor effect.

It is hoped that such an innovative design will inspire further research in fabricating novel efficient nanoparticles for the delivery/separation of biomolecules.

Experimental Section

Chemicals and materials

$\{Mo_{72}Fe_{30}\}$ was synthesized according to a previous publication.[18] Dihexadecyldimethylammonium bromide (97%, $(C_{16}H_{33})_2(CH_3)_2N^+Br^-$, and iron trichloride (99.9%, $FeCl_3$) were purchased from J&K Chemical Co. Ltd, China. The double-chain Mag-Surf, $(C_{16}H_{33})_2(CH_3)_2N^+[FeCl_3Br]^-$, was synthesized by mixing equal molar amounts of $(C_{16}H_{33})_2(CH_3)_2N^+Br^-$ and $FeCl_3$ in methanol and stirring overnight at room temperature, then the solvent was removed, and the product was dried at 80°C, yielding light brown (dark yellow) solids. DNA (Deoxyribonucleic acid from herring sperm, D-3159, < 50 bps) was purchased from Sigma Aldrich. Mb (Myoglobin from equine skeletal Muscle, M0630, 95-100%, essentially salt-free, lyophilized powder) was purchased from Sigma (molar weight is approximately 17 kDa). In all experiments, the concentration of DNA was held constant at 150 $\mu mol \cdot L^{-1}$, and the concentration of Mb was controlled at 10 $\mu mol \cdot L^{-1}$. Each sample of the

complex was prepared by adding appropriate amounts of biomacromolecules, virus-shaped spheres and thrice-distilled water to a fixed volume.

Sample preparation

Initially, a series of solutions of $\{Mo_{72}Fe_{30}\}$ in water and $(C_{16}H_{33})_2(CH_3)_2N^+[FeCl_3Br]^-$ in $CHCl_3$-CH_3OH (3:1, v:v) mixed solvent with gradient concentration were prepared for comparison and optimization. To list an example, $\{Mo_{72}Fe_{30}\}$ was varied from 2, 4, 6, 8 to 10 $mg{\cdot}g^{-1}$; $(C_{16}H_{33})_2(CH_3)_2N^+[FeCl_3Br]^-$ in $CHCl_3$-CH_3OH solvent from 0.50, 0.75, 1.00, 1.25 to 1.50 $mg{\cdot}g^{-1}$. Finally and typically, 8 $mg{\cdot}g^{-1}$ $\{Mo_{72}Fe_{30}\}$ aqueous solution and 1.25 $mg{\cdot}g^{-1}$ $(C_{16}H_{33})_2(CH_3)_2N^+[FeCl_3Br]^-$ in $CHCl_3$-CH_3OH organic solution were selected. The virus-shaped spheres were fabricated as follows: Specifically, 200 μL of 8 $mg{\cdot}g^{-1}$ $\{Mo_{72}Fe_{30}\}$ aqueous solution was gently dropped into 800 μL of 1.25 $mg{\cdot}g^{-1}$ $(C_{16}H_{33})_2(CH_3)_2N^+[FeCl_3Br]^-$ in $CHCl_3$-CH_3OH mixture solvent. A distinct interface was observed between these two liquids initially, then a process of gradual phase re-separation was noted (over about 10 days) until an equilibrium was achieved. The lower phase gradually gave an evident color transition from light yellow (II) to colorless (IV) with its volume fraction becoming smaller. In contrast, the light yellow upper phase (I) formed dark yellow (III) with its volume proportion larger.

Characterization

The spherical aggregates were analyzed by dynamic light scattering (DLS), using a Brookhaven BI-200SM instrument. The measurements were performed at a

scattering angle of 90º using a 200 mW green laser (λ = 532 nm) with variable intensity. The intensity-intensity time correlation functions were analyzed by the CONTIN method. The light scattering cells were rinsed with distilled acetone and ethanol, and then fully dried before use.

The zeta potentials (ξ) of the samples were measured with a Zeta PALS potential analyzer instrument (Brookhaven, USA). It has parallel-plate platinum black electrodes with a 5 mm spacing and a 10 mm path length rectangular organic glass cell. All samples were measured using a sinusoidal voltage of 80 V with a frequency of 3 Hz.

The Small-angle x-ray diffraction (XRD) patterns were acquired on a DMAX-2500PC diffractometer with Cu Kα radiation (λ = 0.15418 nm) and a graphite monochromator. The samples were examined within 1 - 8º in the 2θ mode at 1º min^{-1}.

Freeze dried samples were loaded in sealed polypropylene tubes and fixed inside a plastic straw for measuring in a magnetometer with a superconducting quantum interference device (SQUID, MPMSXL, Quantum Design, San Diego, CA) and a reciprocating sample option (RSO). The experiments were performed at 300 K.

Transmission electron microscopy (TEM) images were acquired on a JEOL JEM-1400 transmission electron microscope (TEM) (acceleration voltage, 120 kV) with a Gatan multiscan charge-coupled device (CCD) for collecting and processing Digital Micrographs.

Scanning electron microscopy (SEM) images were acquired using JEOL JSM6700F and Hitachi S-4800 field-emission scanning electron microscopes. EDS

was performed with a Horiba EMAX-2000 EDS system attached to the SEM microscope. Elemental distribution mapping was carried out using a Hitachi S-4800 microscope.

Atomic force microscopy (AFM) images are undertaken on a Veeco Nanosope IIIa scanning probe microscope operating in tapping mode.

UV-vis measurements were carried out using a U-4100 UV-vis spectrophotometer using a 10 mm path length quartz cell.

FT-IR spectra were recorded on a VERTEX-70/70v FT-IR spectrometer (Bruker Optics, Germany).

Circular dichroism (CD) spectra were performed on a JASCO J-810 spectropolarimeter. Samples were contained in 10 mm path length cells, and the scanning speed was controlled to be 100 nm min^{-1} with the measuring range from 220 to 330 nm. Three scans were averaged per spectrum to improve the signal-to-noise ratio.

Contact angle (CA) measurements are measured on a contact-angle system Kruss DSA (Germany) at room temperature. A drop of ultrapure water (2 μL) was dropped onto the prepared surface. The average CA value was obtained by three repetitive measurements.

X-ray photoelectron spectrometry (XPS) measurements were carried out on ESCALAB 250 X-ray photoelectron spectrometer with a $Mg_{K\alpha}$ excitation source of 10^6 Pa and a resolution of 1.00 eV.

In order to determine specific surface area, N_2 adsorption/desorption experiments

were undertaken on a Quadra-Sorb S at 77.6 K. The sample was out-gassed at 30 ^{o}C under vacuum for 4 h before measurement.

Agarose gel electrophoresis (AGE) was undertaken in agarose gels (2% w/vol). Agarose (2 g) was dissolved in 100 mL 1×tris-acetate-EDTA(TAE) buffer (pH = 8.2) by heating until boiling. Agarose gels (2% w/vol) were formed by cooling the boiling agarose solution to room temperature in a 10×20 cm gel tank. Then, 10 μL DNA containing complex solutions mixed with 2 μL loading buffer were loaded into the holes of the prepared 2% agarose gel horizontally submerged in 1×tris-acetate-EDTA(TAE) buffer (pH = 8.2). Agarose gel electrophoresis was performed at 120 V for 30 min by the JY600C instrument with a standard DNA ladder of 100-700 bps as a reference. After electrophoresis, the gel was developed with ethidium bromide (0.5 $\mu g \cdot mL^{-1}$) and viewed on an UV-vis transilluminator.

Results and Discussion

Interfaces[26] are interesting platforms for the formation of new self-assembled materials. To achieve fabrication of the nanosized vehicles mentioned above, a phase re-separation process at the interface of two distinct liquid phases is developed. As shown in Scheme 1a and Figure S2 (Supporting Information), by simply mixing these two solutions (the upper phase must be gently dropped onto the lower phase without too much mixing), an obvious interfacial mass exchange can be observed even with the naked eye at the interface. Then a process of gradual phase re-separation of these two liquids is observed over time (see Supporting Video). The lower phase gradually undergoes an evident color transition from light yellow (phase II) to colorless (phase

IV) with its volume fraction becoming smaller. In contrast, the light yellow upper phase (phase I) turns dark yellow (phase III) and its volume fraction becomes larger. That is, both methanol and $(C_{16}H_{33})_2(CH_3)_2N^+[FeCl_3Br]^-$ in II phase merges into the upper phase III driven by strong electrostatic interactions (between negative $\{Mo_{72}Fe_{30}\}$ and positive $(C_{16}H_{33})_2(CH_3)_2N^+$ and the like dissolves like principle, since methanol is more soluble in water). The combined effects of strong electrostatic interactions, interfacial exchange and the like dissolves like principle play important roles in this process. A mixed solvent of chloroform and methanol is employed in phase II because fast evaporation of pure chloroform can lower the system stability, or even result in layer fusion. Addition of methanol boosts the hydrophobic interaction between the alkyl chains, thereby enhancing the stability of the aggregates.[21]

Robust spherical vesicles and their fusion

TEM (Figure 1a) and AFM (Figure 1d) observations indicate that vesicles (hollow spherical assemblies) with diameters ranging from 100 to 900 nm formed in a very short time (3 min) after the upper phase is gently dropped onto the lower phase. Visible mass transport at the interface can be seen by the naked eye (see Supporting Video). The membrane thicknesses of the vesicles captured by TEM images range from 18 nm (4 layers) to 98 nm (22 layers), as shown by a statistical distribution of membrane thickness (Figures S3 and S4, Supporting Information). A possible onion-like vesicle structure composed of a multi-layer structure is proposed, as shown in Scheme 1a. Wu et al. also found similar structures in

POM/surfactant systems.[27] Unexpectedly and interestingly, a process of hierarchical assembly[28] takes place over time, namely, the spheres gradually grow both in quantity and size (Figure 1b and 1e) until adhesion and fusion occur, as shown in Figure 1c and Figure 1f and 1g. As can be seen in Figure 1h and 1i, TEM and SEM images show that the vesicles undergo a gradual aggregation, forming secondary-assemblies. In the first stage, two individual vesicles collide and experience cohesion and fusion, then this process is enhanced by attachment and aggregation of numerous smaller subsidiary spheres. It should be noted that, during this process, two similar but different routes (fusion and cohesion) co-exist, as shown in Scheme 1b. This is probably because that the local concentrations at different sites of the interface are different; consequently, the mass transport (exchange) rates are also different at different sites. The key to this process is the gentle adding of two phases and slow initiation of the phase re-separation. Clearly, the formation of the virus-shaped vesicle complexes is a dynamic process. As the quantities of independent vesicles increase, the original larger vesicles dissociate and re-self-assemble, and the virus-shaped vesicles gradually dominate in the system. Generally, vesicles formed by amphiphilic molecules can be destabilized once they are taken out of water (or after solvent evaporation).[29] Herein, robust hybrid vesicles are formed by amphiphilic compounds with the assistance of POMs, which improves the structural integrity, and thus could further expand application of the complexes.

Virus-shaped spheres

Over 10 days during the phase re-separation process, SEM and AFM

observations were used to study the aggregate morphology in the upper phase. The SEM (Figure 2a, 2b and 2c) and TEM (Figure 2d) images reveal the presence of virus-shaped spheres composed of smaller spheres with diameters ranging from 100 nm to 800 nm. The morphologies are reminiscent of viruses (inset of Figure 2c, thus they are denoted virus-shaped spheres). An AFM image (Figure 2e), taken in tapping mode, further shows that the spheres are composed of smaller subsidiary spheres. An AFM height image (Figure 2f) and cross-sectional analysis (Figure 2g and 2h) indicate that the virus-shaped spheres have uneven surfaces. With the loss of solvent, the spheres tend to appear flatter when dried on the substrate. It is noted that the height of the virus-shaped spheres is less than 70 nm, smaller than their horizontal diameters, confirming that the interiors of the virus-shaped spheres are hollow. Energy-dispersed X-ray spectroscopy (EDS) analysis was used to probe the chemical composition of virus-shaped particles (Figure 2i). The presence of Mo, Fe, O, C, Cl and Br was detected. The Mo, Fe, O signals may have originated from $\{Mo_{72}Fe_{30}\}$ (Fe also from surfactant), and C, Cl and Br from $(C_{16}H_{33})_2(CH_3)_2N^+[FeCl_3Br]^-$. These results provide strong evidence that mixed complexes are formed, in accordance with the composition of components.

X-ray photoelectron spectroscopy (XPS) was also employed to analyze the surface chemical composition of these virus-shaped spheres (Figure S5a-S5d, Supporting Information), confirming the presence of Fe, C, N, Mo, Cl and Br. Peaks corresponding to Br 3d (BE = 69.2 eV), Mo 3d5/2 (BE = 232.9 eV) and Fe

2p3/2 (BE = 711.2 eV) were detected, and the Br 3d signals can be assigned to the Mag-Surf $(C_{16}H_{33})_2(CH_3)_2N^+[FeCl_3Br]^-$, whereas the Mo 3d and Fe 2p are ascribed to $\{Mo_{72}Fe_{30}\}$ POMs. XPS results again confirm the presence of $(C_{16}H_{33})_2(CH_3)_2N^+[FeCl_3Br]^-$ and $\{Mo_{72}Fe_{30}\}$ in the virus-shaped complexes, supporting the results. Elemental maps show a uniform distribution of these elements over micron scales (Figure S5e, Supporting Information). In particles, C, Cl, O, Mo and Fe are uniformly distributed and correlate with shape in the sample area.

Additionally, small angle X-ray diffraction (XRD) patterns of the dry virus-shaped spheres are consistent with a lamellar structure, and a layer spacing of about 4.42 nm (Figure 3A), which is consistent with the TEM images, namely, the virus-shaped spheres are composed of smaller subsidiary spheres. As the Mag-Surf $(C_{16}H_{33})_2(CH_3)_2N^+[FeCl_3Br]^-$ has a calculated extended chain length (L) of 2.17 nm[30] and $\{Mo_{72}Fe_{30}\}$ has a diameter (d) of ca. 2.5 nm,[31] a possible scenario is that the surfactant chains are compressed in the aggregates, which is consistent with the FT-IR results (Figure 3B).

The complexes were used to coat a glass slide, and the contact angle of water droplets was measured. The resulting static contact angle was 39º (Figure 3C), suggesting that the aggregate exteriors consist of hydrophilic positively charged head-groups of $(C_{16}H_{33})_2(CH_3)_2N^+$. The counter-ion $[FeCl_3Br]^-$, due to its magnetic[32] and hydrophobic characteristics,[33] is expected to associate strongly on the periphery of $\{Mo_{72}Fe_{30}\}$ and among the hydrophobic alkyl chains of $(C_{16}H_{33})_2(CH_3)_2N^+$. Of course, the counter-ion $[FeCl_3Br]^-$ will not appear in the exterior of the overall

aggregates due to its hydrophobicity,[33] which can be confirmed by the positive zeta-potential (ξ = 37.06 mV).

To gain insight into the mechanism of formation of these virus-shaped assemblies, the assemblies were investigated at different stages. {$Mo_{72}Fe_{30}$} is a large macro-anion in aqueous solution, the positive hydrophilic head-groups of $(C_{16}H_{33})_2(CH_3)_2N^+$ are reasonably expected to be electrostatically attracted to {$Mo_{72}Fe_{30}$} and {$Mo_{72}Fe_{30}$} encapsulated by $(C_{16}H_{33})_2(CH_3)_2N^+$ (Scheme 1a). In phase III, the alkyl chains will segregate from the aqueous sub-phase driven by hydrophobic forces, then the rearrangement[21] of $(C_{16}H_{33})_2(CH_3)_2N^+$ cations on the exterior of {$Mo_{72}Fe_{30}$} POMs will lead to the formation of spherical assemblies. The morphology of the magnetic aggregates undergoes three stages of development, which can be confirmed by the zeta potential ξ values (Figure 4a). An increase of ξ follows the formation of the virus-shaped spheres. In the first 1 min, layered hollow vesicles are evidenced by the half-cut spheres in SEM images (first inset in Figure 4a). During the initial stage, the system undergoes rapid mass transport (exchange) and has low colloidal/kinetic stability (ξ = 2.38 mV). In the second stage (within about 60 min), the hollow spheres become plump and complete, some spheres begin to adhere and fuse, and ξ increases. In the last stage (around 10 days), the spheres become saturated and re-aggregate into more and more virus-shaped clusters. At this time, the virus-shaped spheres are uniform and relatively evenly distributed (Figure 2a). After around 10 days, phase III turns dark yellow and its volume becomes larger (Scheme 1a). At this time, phase III containing

virus-shaped aggregates is colloidal/kinetically stable (ξ = 37 mV) and exhibits a strong Tyndall effect (inset of Figure 4b), indicating the existence of colloidal-size particles. DLS data clearly demonstrate the existence of aggregates with an average diameter of 900 nm, and a size distribution ranging from 600 to 1400 nm (Figure 4b).

It should be noted that, after phase re-separation, the aggregates are not static since they are in a process of dynamic mass transport. During the formation process, the larger core shell spheres form first, followed by attachment of the smaller subsidiary hollow shell spheres. The originally formed spheres may collapse and reform into more complicated virus-shaped spheres, due to concentration saturation and the high affinity of the small spheres for each other (electrostatic and hydrophobic interactions). Such an abundance of nanosized aggregates has a strong tendency to precipitate from the bulk. After 30 days, the virus-shaped spheres aggregate into sediments and spread along the interface, which can be seen by the naked eye. It appears there is a time-dependent fabrication of magnetic/electrostatic complexes. SQUID magnetometry (Figure 4c) demonstrates that the virus-shaped spheres show typical paramagnetism. A negligible hysteresis loop can be captured in Figure 4c, indicating faint ferromagnetism, thus the spheres can be magnetized and attracted by external magnetic fields.

The virus-shaped spheres are not only colloidal/kinetically stable (ξ = 37 mV), but also combine relatively high-ferro-magnetism and high-specific-surface- area/positive charge-rich surfaces together. The positively charged surfaces may have potential for attracting and capturing negative biomolecules like DNA and proteins, the magnetic

properties may then afford spatial control by applying magnetic fields, which is demonstrated below.

Anchor and motor

The electric charge of the virus-shaped spheres is derived from all the spheres composing it. With a high charge density, the electrostatic interactions between the virus-shaped spheres and biomolecules will be greatly enhanced (consistent with Coulomb's law). These interactions act as an anchor, and magnetism can be considered as a motor driving migration under an applied magnetic field. Previous work has shown that cationic surfactants can compact DNA by association onto DNA backbones.[34] Nanoparticles made of Au/magnetic cationic surfactant complexes can also significantly enhance the compaction efficiency of DNA,[35] and in a similar fashion the complexes introduced here are also expected to compact and migrate DNA. In a modest magnetic field (NdFeB, 0.3T), a certain number of the charge-rich magnetic virus-shaped spheres are expected to bind DNA via electrostatic interaction and migrate to the magnet (Scheme 1c). Because DNA has a characteristic absorbance band at 260 nm,[36] the DNA concentration can be monitored over time by UV-vis absorbance at 260 nm. For better observation of the concentration of DNA or Myoglobin molecules, the other interferences must be excluded. A typical UV-vis spectrum of the magnetic virus-shaped spheres phase III is shown in Figure S6 (Supporting Information), and an overlap in UV-vis spectrum can be seen in the range from 200 nm to 300 nm. So, dilution of the magnetic virus-shaped complexes was carried out to better monitor the biomolecules via

UV-vis spectroscopy. A series of dilution ratios were tested (Table S1, Supporting Information), from which the critical interaction concentration between the virus-shaped spheres and DNA was between 3.71 and 4.24 μmol·L^{-1} (with respect to $(C_{16}H_{33})_2(CH_3)_2N^+[FeCl_3Br]^-$ moiety). At high concentration of virus-shaped spheres (84.8 μmol·L^{-1}), DNA (150 μmol·L^{-1}) has a 95% decrease within 24 hrs in concentration as shown in Figure S7 (Supporting Information), exhibiting good DNA absorption ability of virus-shaped spheres. At low concentration (3.71 μmol·L^{-1}) near the critical interaction concentration, the virus-shaped spheres facilitated a magnetic field-motored transport and enrichment of DNA. The morphology and size of the magnetic complexes after dilution (3.71 μmol·L^{-1}) was maintained (Figure S8, Supporting Information), rather than any destabilization owing to dilution. When mixing 3.71 μmol·L^{-1} magnetic spheres and DNA (150 μmol·L^{-1}) in the absence of magnetic field, UV-vis spectroscopy (Figure S9, Supporting Information) demonstrates a negligible reduction in intensity at 260 nm. More importantly, no evidence of reduction in absorption was observed over 96 hr, indicating that no obvious aggregation occurs owing to interaction of virus-shaped complexes with DNA. In an applied magnetic field (0.3 T), magnetic virus-shaped particles show a directional migration, and thus increase the local concentration in the vicinity of the magnet, leading to the capture and transport of DNA onto the magnet surface. A notable decrease in DNA concentration of 68% was observed over 96 hr, as shown by UV-vis (Figure 5a) and circular dichroism (CD) spectra (Figure 5b). It is worth noting that migration in the magnetic field increases the local concentration of the magnetic

virus-shaped sphere/DNA complexes adjacent to the magnet, so that it exceeds the solubility limit. Noticeable aggregation can be seen on the surface of the magnet (inset in Figure 5a). Phase separation (precipitates) indicates DNA compaction and association due to the relief of charge repulsion between adjacent DNA backbones.[36]

CD can be utilized to better trace the targeted migration of DNA. The CD spectroscopy of DNA (Figure 5b) shows the characteristic negative band peak at 242 nm owing to the helicity of DNA and a positive band peak at 275 nm due to base stacking.[37] In the presence of an applied magnetic field (NdFeB magnet, 0.3 T), the two characteristic band peaks show a remarkable decrease in intensity, suggesting a decrease of DNA concentration. It is noted that the negative band peak, indicating the secondary structure of DNA,[35,38] exists persistently throughout the transport process. This process demonstrates that DNA retains its native β-form during the migration, i.e., the virus-shaped complexes act as effective delivery vehicles without damaging the native conformation of DNA.

Agarose gel electrophoresis results permit to follow a time-dependent compaction of DNA in an applied magnetic field as shown in Figure 5c. SEM elemental mapping (Figure 5d) was conducted during the magnetic delivery process. The presence of Mo, Cl and P on the spheres indicates that DNA uniformly distributed on the surface of the magnetic spheres (Figure 5d). An EDS spectrum (Figure S10, Supporting Information) also gives evidence to support presence of DNA. Addition of sufficient NaBr as a background electrolyte can screen the

electrostatic interactions between DNA and the virus-shaped particles, thus leading to the release of DNA, as shown by the CD spectra (Figure S11, Supporting Information). The characteristic band peaks of DNA almost recover without significant variation either in position or intensity. Thus, this combined nano-anchor and -motor approach can be well utilized to capture and release DNA, i.e., concentrating and separating without destroying functionality.

The targeted migration applications are not only limited to DNA, but are also demonstrated with a model protein myoglobin (Mb) (Figure 5e-5g). A mixture of 10 $\mu mol \cdot L^{-1}$ Mb and 8.48 $\mu mol \cdot L^{-1}$ magnetic virus-shaped sphere complexes also undergoes magnetically-induced migration. In the UV spectrum, Mb/magnetic virus-shaped sphere complexes exhibit a strong characteristic Soret band at 409 nm, and Q_a, Q_b bands at 641 nm and 502 nm, respectively. These three band peaks suggest myoglobin with a diamagnetic (low-spin) heme group as well as a six-coordinate geometry with a strongly bound water molecule.[39] Both in the absence and presence of a magnetic field, UV-vis spectra of 10 $\mu mol \cdot L^{-1}$ Mb in the presence of an external magnetic field do not change over time (Figure 5f), suggesting aggregations and migration are not observed. However, in the presence of an applied magnetic field, UV-vis spectra of 10 $\mu mol \cdot L^{-1}$ Mb/8.48 $\mu mol \cdot L^{-1}$ magnetic complex show a notable reduction over 96 hr (Figure 5e). Approximately 73% of Mb (based on the UV data 27% remained in the bulk solution) are concentrated and migrated to the vicinity of the magnet, leading to brown precipitates (Figure 5g).

Surfactants interact with proteins, such as Mb, in multifarious ways, including

strong binding to the charged and hydrophobic side chains of proteins[40] bringing about difficulties for delivery and separation of proteins,[35] especially denaturation. Addition of anionic surfactants[41] or magnetic nanoparticles (coated by cationic surfactant)[35] to Mb is not expected to result in denaturation; interestingly similar results are obtained for the systems here. The introduction of virus-shaped spheres does not shift the characteristic peak position for Mb, excluding distinct changes in the tertiary structure in the vicinity of the heme group[31] or denaturation during the magnetic motored transporting process.

Conclusions

In summary, the newly synthesized double-tailed Mag-Surf $(C_{16}H_{33})_2(CH_3)_2N^+[FeCl_3Br]^-$ generates virus-shaped hybrid assemblies with polyoxometalate $\{Mo_{72}Fe_{30}\}$, these nanostructures can be utilized for binding, anchoring and delivery of biomolecules, such as DNA. The main advance of over other approaches for the time-dependent formation of hollow shell structures is the increase in magnetic effect owing to the unique combination magnetic surfactants, and also demonstrate that the hollow shell structures fabricated using a dynamic interfacial process are new findings in colloid and interface science. As an interesting nano-anchor and -motor system, the virus-shaped spheres are not only colloidal/kinetically stable, but also combine relatively high-ferro-magnetism, high-specific-surface-area and positive charge-rich surfaces together. The high charge nature of the complex surfaces can attract and capture bio-molecules like DNA (95% DNA absorption capacity

within 24 hr) and a model protein myoglobin even at low strength magnetic fields. This method provides a gentle easy way to fabricate nano-scale magnetic complex materials, offering a potential application for capture and separation, including for biomolecules.

Supporting Information

Supporting Information is available from the Wiley Online Library or from the author.

Acknowledgements

This work was funded by the National Natural Science Foundation of China (Grant Nos. 21420102006).

Conflict of Interest

The authors declare no conflict of interest.

Received: ((will be filled in by the editorial staff))

Revised: ((will be filled in by the editorial staff))

Published online: ((will be filled in by the editorial staff))

References

1. Chen C, Chen W, Lu J, Chu D, Huo Z, Peng Q, Li Y, Transition-metal phosphate colloidal spheres. *Angew Chem Int Ed.* 2009; 48: 4816-4819.
2. Polshettiwar V, Cha D, Zhang X, Basset JM, High-surface-area silica nanospheres (KCC-1) with a fibrous morphology. *Angew Chem Int Ed.* 2010; 49: 9652-9556.
3. Burns JR, Göpfrich K, Wood JW, V. V. Thacker, E. Stulz, U. F. Keyser, S. Howorka, Lipid-bilayer-spanning DNA nanopores with a bifunctional porphyrin

anchor. *Angew Chem Int Ed.* 2013; 52: 12069-12072.

4. Cui J, Rose RD, Best JP, Johnston, APR, S. Alcantara, K. Liang, G. K. Such, S. J. Kent, F. Caruso, Mechanically tunable, self-adjuvanting nanoengineered polypeptide particle. *Adv Mater.* 2013; 25: 3468-3472.
5. Coelho JP, González-Rubio G, Delices A, Barcina JO, Salgado C,Ávila D, Peña-Rodríguez O, Tardajos G, Guerrero-Martínez A, Polyrotaxane-mediated self-assembly of gold nanospheres into full reversible supercrystals. *Angew Chem Int Ed.* 2014; 53: 12751-12755.
6. Upert G, Bouillère F, Wennemers H, Oligoprolines as scaffolds for the formation of silver nanoparticles in defined sizes: correlating molecular and nanoscopic dimensions. *Angew Chem Int Ed.* 2012; 51: 4231-4234.
7. Yang Z, Altantzis T, Zanaga D, Bals S, Tendeloo GV, Pileni MP, Supracrystalline colloidal eggs: epitaxial frowth and freestanding three-dimensional supracrystals in nanoscaled colloidosomes. *J Am Chem Soc.* 2016; 138: 3493-3500.
8. Yu C, Zhang J, Granick S, Selective janus particle assembly at tipping points of thermally-switched wetting. *Angew Chem Int Ed.* 2014; 53: 4364-4367.
9. Fang Y, Zheng G, Yang J, Tang H, Zhang Y, Kong B, Lv Y, Xu C, Asiri AM, Zi J, Zhang F, Zhao D, Dural-pore mesoporous carbon@silica composite core-shell nanospheres for multidrung delivery. *Angew Chem Int Ed.* 2014; 53: 5366-5370.
10. Sun T, Zhang YS, Pang B, Hyun DC, Yang M, Xia Y, Engineered nanoparticles for drug delivery in cancer therapy. *Angew Chem Int Ed.* 2014; 53: 12320-12364.
11. Qian Q, Huang X, Zhang X, Xie Z, Wang Y, One-step preparation of macroporous

polymer particles with multiple interconnected chambers: a candidate for trapping biomacromolecules. *Angew Chem Int Ed.* 2013; 52: 10625-10629.

12. Kay ER, Leigh DA, Zerbetto F, Synthetic molecular motors and mechanical machnies. *Angew Chem Int Ed.* 2007; 46: 72-191.
13. Malakoutikhah M, Teixidó M, Giralt E, Shuttle-mediated drug delivery to the brain. *Angew Chem Int Ed.* 2011; 50: 7998-8014.
14. Liao J, Zhu Y, Zhou Z, Chen J, Tan G, Ning C, Mao C, Reversibly controlling preferential protein adsorption on bone implants by using an applied weak potential as a switch. *Angew Chem Int Ed.* 2014; 53: 13068-13072.
15. Samanta A, Ravoo BJ, Magnetic separation of proteins by a self-assembled supramolecular ternary complex. *Angew Chem Int Ed.* 2014; 53: 12946-12950.
16. Brown P, Bushmelev A, Butts CP, Cheng J, Eastoe J, Grillo I, Heenan RK, Schmidt AM, *Angew Chem Int Ed.* 2012; 51: 2414-2416.
17. Dias RS, Lindman B, Miguel MG, Compaction and decompaction of DNA in the preence of catanionic amphiphile mixtures. *J Phys Chem B.* 2002; 106: 12608-12612.
18. Müller A, Luban M, Schröder C, Modler R, Kögerler P, Axenovich M, Schnack J, Canfield P, Bud'ko S, Harrison N, Classical and quantum magnetism in giant Keplerate magnetic molecules. *ChemPhysChem* 2001; 2: 517-521.
19. Li X, Gao Y, Boott CE, Hayward DW, Harnima R, Whittell GR, Richardson RM, Winnik MA, Manners I, "Cross" supermicelles via the hierarchical assembly of amphiphilic cylindrical triblock comicelles. *J Am Chem Soc.* 2016; 138:

4087-4095.

20. Rädler J, Radmacher M, Gaub HE, Velocity-dependment forces in atomic force microscopy imaging of lipid films. *Langmuir* 1994; 10: 3111-3115.
21. Tanford C, Micelle shape and size. *J Phys Chem.* 1972; 76: 3020--3024.
22. Fan D, Jia X, Tang P, Hao J, Liu T, Self-patterning of hydrophobic materials into highly ordered honeycomb nanostructures at the air/water interface. *Angew Chem Int Ed.* 2007; 46: 3342-3345.
23. Zhao W, Dong S, Hao J, Colloidal wormlike micelles with highly ferromagnetic properties. *Langmuir* 2015; 31: 11243-11248.
24. Brown P, Bushmelev A, Butts CP, Eloi JC, Grillo I, Baker PJ, Schmidt AM, Eastoe J, Properties of new magnetic surfactants. *Langmuir* 2013; 29: 3246-3251.
25. Müller A, Sarkar S, Shah SQN, Bögge H, Schmidtmann M, Sarkar S, Kögerler P, Hauptfleisch B, Trautwein AX, Schünemann V, Archimedean synthesis and magic numbers: “sizing” giant molybdenum-oxide-based molecular spheres of the keplerate type. *Angew Chem Int Ed.* 1999; 38: 3238-3241.
26. Mel’nikov SM, Sergeyev VG, Yoshikawa K, Discrete coil-globule transition of large DNA induced by cationic surfactants. *J Am Chem Soc.* 1995; 117: 2401-2408.
27. Mel’nikov YS, Lindman B, pH-controlled DNA condensation in the presence of dodecyldimethylamine oxide. *Langmuir* 2000; 16: 5871-5878.
28. Kim S, Bellouard C, Eastoe J, Canilho N, Rogers SE, Ihiawakrim D, Ersen O, Pasc A, Spin state as a probe of vesicle self-assembly. *J Am Chem Soc.* **2016;** *138:*

2552-2555.

29. Brown P, Khan AM, Armstrong JPK, Perriman AW, Butts CP, Eastoe J, Magnetic DNA and proteins using responsive surfactants. *Adv. Mater.* **2012;** *24:* 6244-6247.

30. Izzet G, Abécassis B, Brouri D, Piot M, Matt B, Serapian SA, Bo C, Proust A, Hierarchical self-assembly of polyoxometalate-based hybrids driven by metal coordination and electrostatic interactions: from discrete supramolecular species to dense monodisperse nanoparticles. *J Am Chem Soc.* 2016; 138: 5093-5099.

31. Long D, Tsunashima R, Cronin L, Polyoxometalates: building blocks for functional nanoscale systems. *Angew Chem Int Ed.* 2010; 49: 1736-1759.

32. Wang F, Seo JH, Luo G, Starr MB, Li Z, Geng D, Yin X, Wang S, Fraser DG, Morgan D, Ma Z, Wang X, Nanometre-thick single-crystalline nanosheets grown at the water-air interface. *Nat Commun.* **2016**; *7:* 10444-10451.

33. Li H, Sun H, Qi W, Xu M, Wu L, Onionlike hybrid assemblies based on surfactant-encapsulated polyoxometalates. *Angew Chem Int Ed.* 2007; 46: 1300-1303.

34. Ny ALML, Lee CTJr, Photoreversible DNA condensation using light-responsive surfactants. *J Am Chem Soc.* 2006; 128: 6400-6408.

35. Xu L, Feng L, Dong S, Hao J, Magnetic controlling of migration of DNA and proteins using one-step modified gold nanoparticles. *Chem Commun.* 2015; 51: 9257-9260.

36. Carlstedt J, Lundberg D, Dias RS, Lindman B, Condensation and decodensation

of DNA by cationic surfsactant, spermine, or cationic surfactant-cyclodextrin mixtures: macroscopic phase behacior, aggregate properties, and dissolution mechanisms. *Langmuir* 2012; 28: 7976-7989.

37. Bonincontro A, Marchetti S, Onori G, Santucci A, Complex formation between DNA and dodecyl-dimethyl-amine-oxide induced by pH. *Chem Phys Lett.* 2003, 370: 387-392.

38. Bonincontro A, Falivene M, Mesa CL, Risuleo G, Peña MR, Dynamics of DNA adsorption on and release from SDS-DDAB cat-anionic vesicles: a multitechnique study. *Langmuir* 2008; 24: 1973-1978.

39. Antonini E, Brunori M, *North-Holland Publishing Company Amsterdam*, London, **1971**.

40. Andersen KK, Westh P, Otzen DE, Global study of myoglobin-surfactant interactions. *Langmuir* 2008; 24: 399-407.

41. Perriman AW, Brogan APS, Cölfen H, Tsoureas N, Owen GR, Mann S, *Nat Chem.* 2010; 2: 622-626.

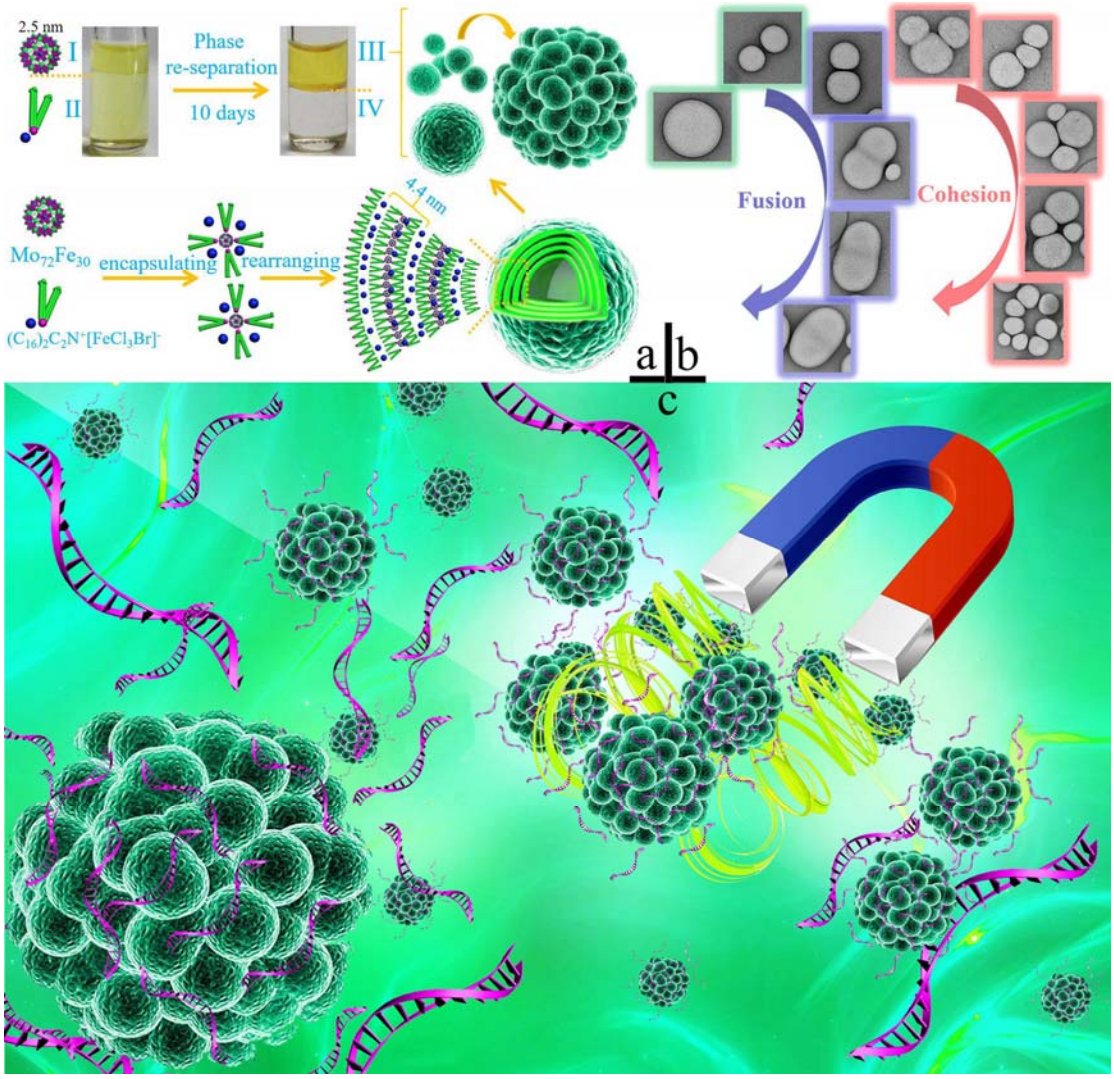

Scheme 1. Schematic illustration of preparation, evolution and biomolecule delivery with virus-shaped spheres. (a) An illustration of the fabrication of virus-shaped spheres by phase re-separation. Notes: I, 200 μL of 8 mg·g^{-1} {$Mo_{72}Fe_{30}$} aqueous solution; II, 800 μL of 1.25 mg·g^{-1} $(C_{16}H_{33})_2(CH_3)_2N^+[FeCl_3Br]^-$ in $CHCl_3$-CH_3OH (3:1, v:v) organic mixture; III, The upper phase after phase re-separation; IV, The lower phase after phase re-separation. (b) Two different evolutionary schematic routines of sphere aggregation (fusion and cohesion) shown by TEM images. **(c)** A cartoon illustrating the virus-shaped spheres transporting target molecules using an applied external magnetic field. Note: for conciseness, only DNA is exhibited in the cartoon.

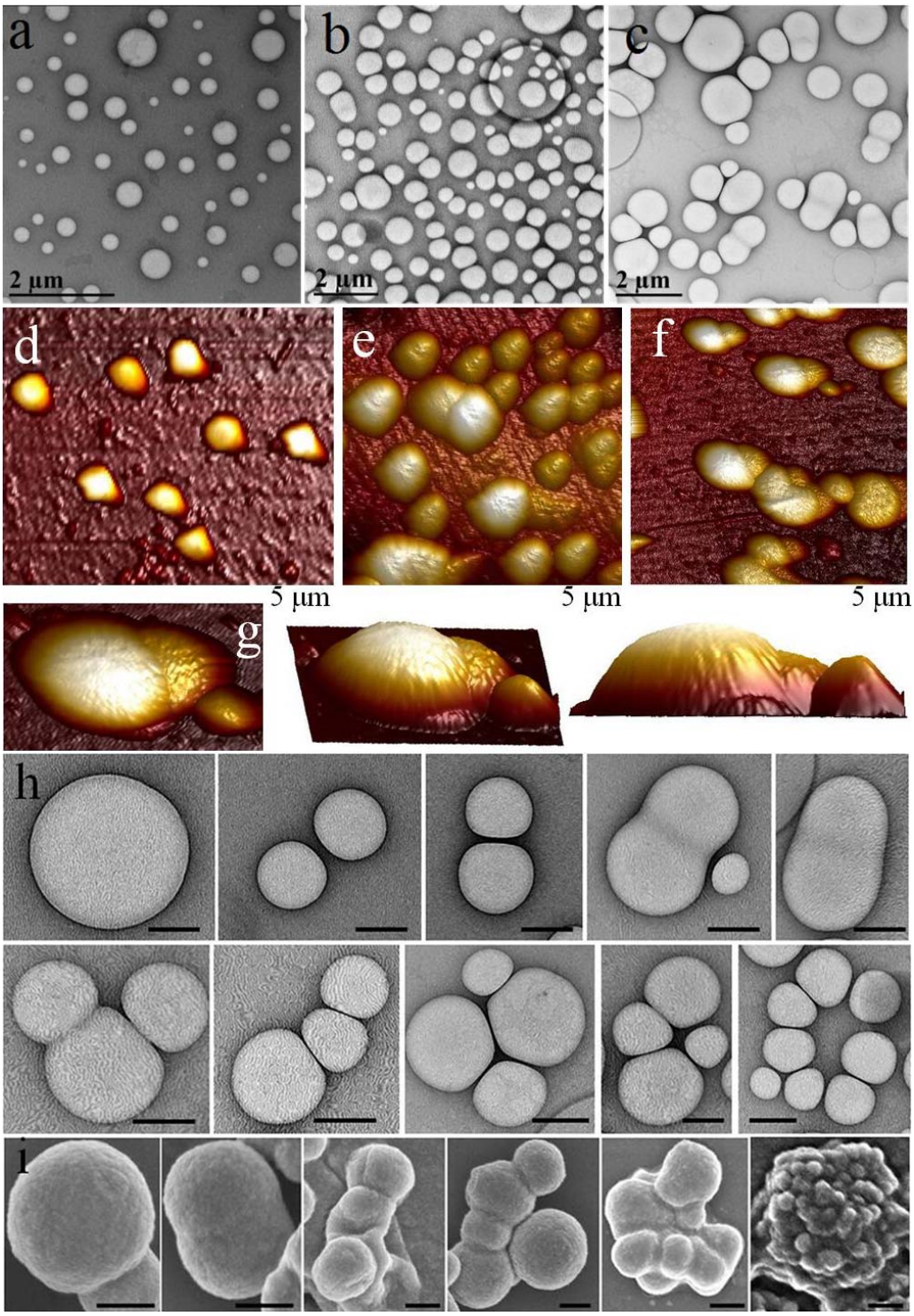

Figure 1. Evolution in morphology of the aggregates in phase III. (a, b, c) TEM images for the aggregates in phase III captured at different times (a, 3 min; b, 10 min; c, 60 min). (d, e, f, g) AFM images for the aggregates in phase III. (d, 3 min; e, 10 min; f and g, 60 min). Development of (h) TEM images and (i) SEM images at longer observation times. The bars in (h) and (i) indicate 200 nm.

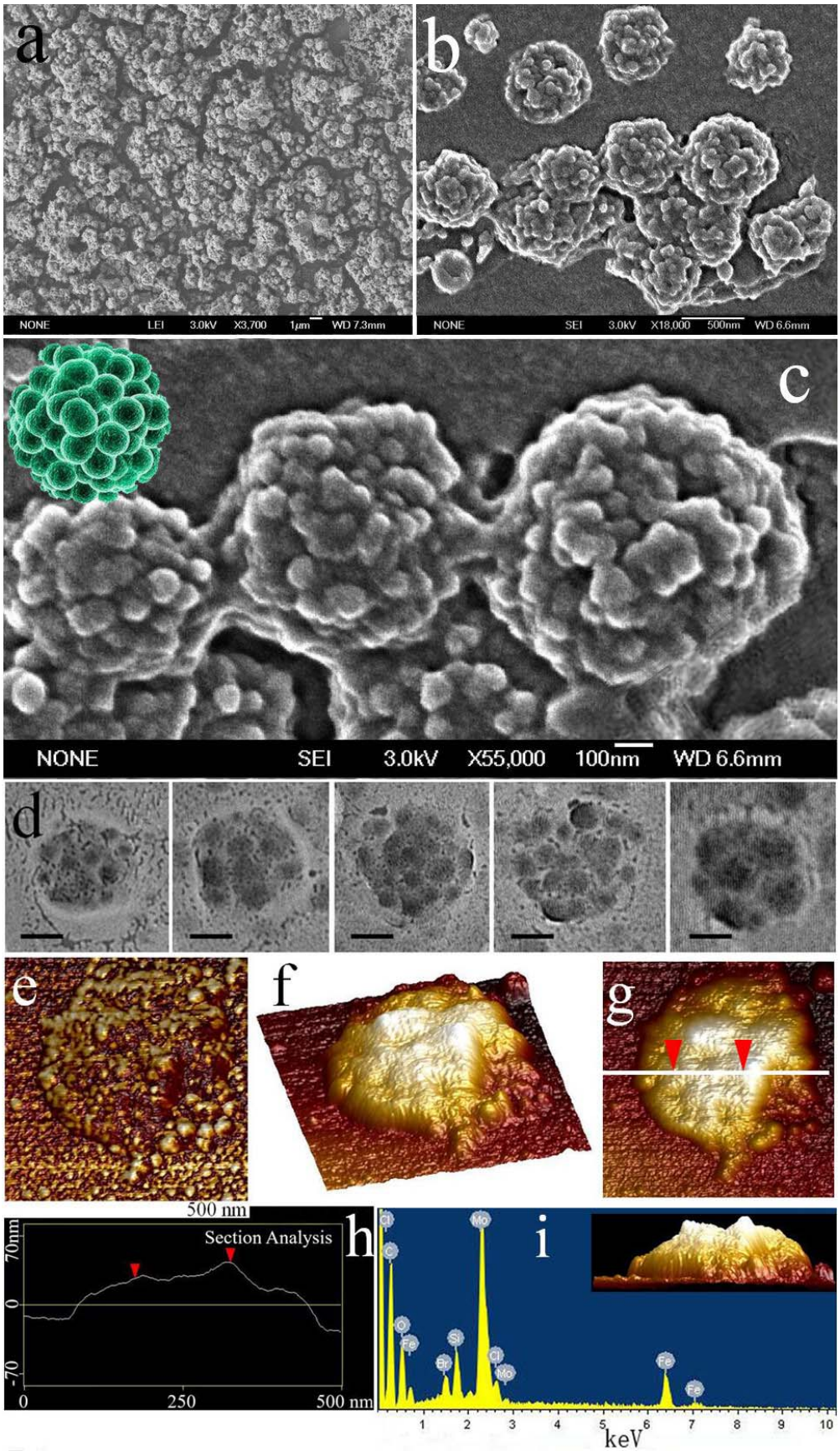

Figure 2. Morphology of virus-shaped spheres. (a, b, c) SEM, (d) TEM (bars: 200 nm) and (e, f, g) AFM images of the aggregates in phase III after 10 days. Inset in (c):

Schematic cartoon images of virus-shaped spheres. (h) Cross section along the line indicated in (g). (i) EDS spectrum revealing the composition of the virus-shaped spheres.

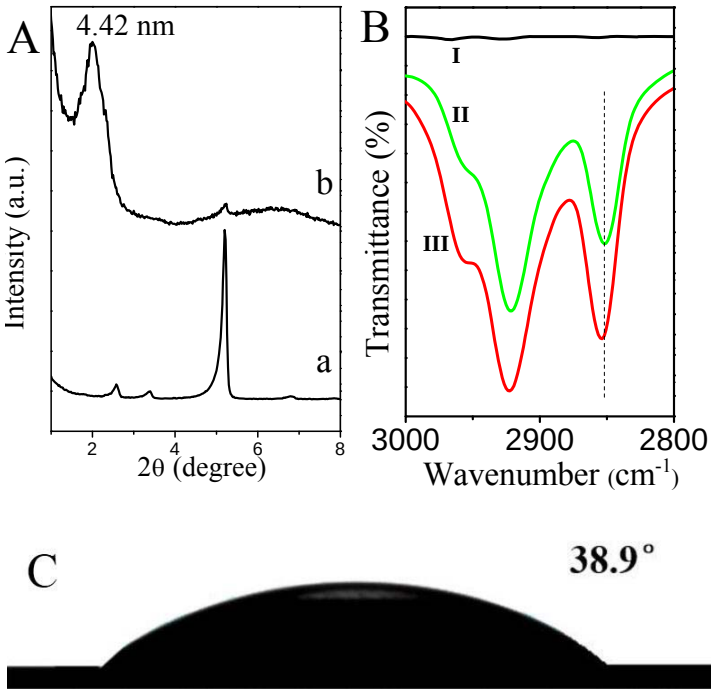

Figure 3. Specific characterization of virus-shape spheres. (A) Small angle X-ray diffraction (XRD) patterns of pure $(C_{16}H_{33})_2(CH_3)_2N^+[FeCl_3Br]^-$ powders (a) and dry virus-shape spheres (b) from the upper phase solution (III). Bragg equation: $2d \sin\theta = \lambda$ (λ = 0.15418 nm). (B) FT-IR spectra of the (I) $\{Mo_{72}Fe_{30}\}$, (II) dry virus-shaped spheres and (III) pure $(C_{16}H_{33})_2(CH_3)_2N^+[FeCl_3Br]^-$ powders. (C) The static contact angle of a covering film of the virus-shape assemblies.

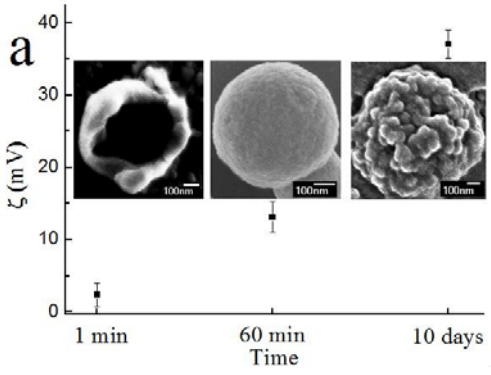

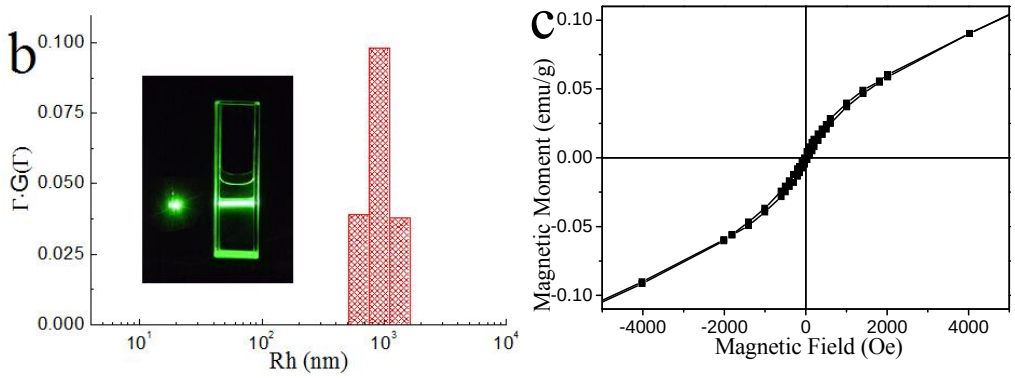

Figure 4. Stabilities, size distribution of virus-shaped spheres and SQUID magnetometry. (a) Zeta potential of phase III at different observing times. Insets are corresponding SEM images. (b) Dynamic light scattering giving particle size distribution using the CONTIN analysis for phase III after 10 days. Inset: Photo showing the Tyndall effect of large colloidal aggregates for phase III. (c) Hysteresis plots for dry aggregates in phase III.

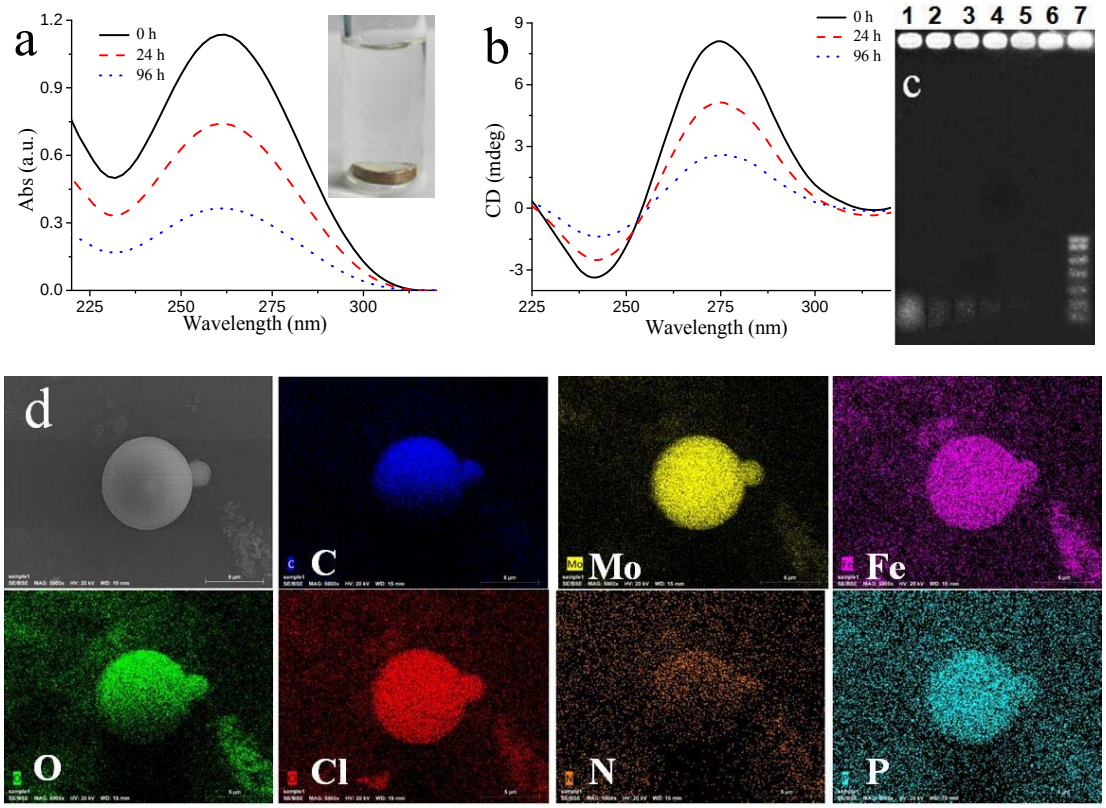

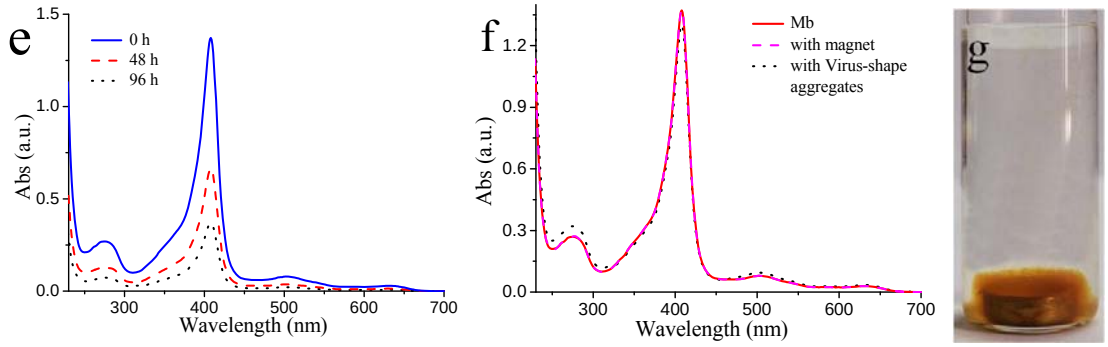

Figure 5. The magnetic delivery of biomolecules. (a) UV-vis spectra and (b) CD spectra of the 150 μmol·L^{-1} DNA/3.71 μmol·L^{-1} magnetic virus-shaped sphere complexes in the presence of an applied magnetic field (NdFeB magnet, 0.3 T) at different times. t = 0 (black solid line), t = 24 hour (dashed line) and t = 96 hour (dotted line). Inset in (a): The migration of DNA induced by the magnetic virus-shaped spheres in the presence of a NdFeB magnet (0.3 T). (c) Agarose gel electrophoresis results of a time-dependent compaction and delivery of DNA in a magnetic field, i.e., upper residual solution of 150 μmol·L^{-1} DNA/3.71 μmol·L^{-1} magnetic virus-shaped sphere complexes mixture with different collecting time with an applied magnetic field. Lane 1 refers to the sample containing free DNA; samples in lanes 2, 3, 4, 5, and 6 are collected from upper residual after the introduction of a magnet for 12, 24, 36, 48, 96 h respectively; lane 7 refers to a DNA molecular weight marker. (d) Elemental mapping of the aggregating spheres after adsorption of DNA. (e) UV-vis spectra of 10 μmol·L^{-1} Mb/8.48 μmol·L^{-1} magnetic virus-shaped sphere complexes with applied magnetic field at different times. t = 0 (black solid line), t = 48 hr (dashed line) and t = 96 hr (dotted line). (f) UV-vis spectra of 10 μmol·L^{-1} Mb without/with an external magnetic field and UV-vis spectra of 10 μmol·L^{-1} Mb/8.48 μmol·L^{-1} magnetic virus-shape sphere complexes without applied magnetic field. (g) The migration of Mb induced by the magnetic virus-shaped spheres in the presence of a NdFeB magnet (0.3 T).

Table of Contents:

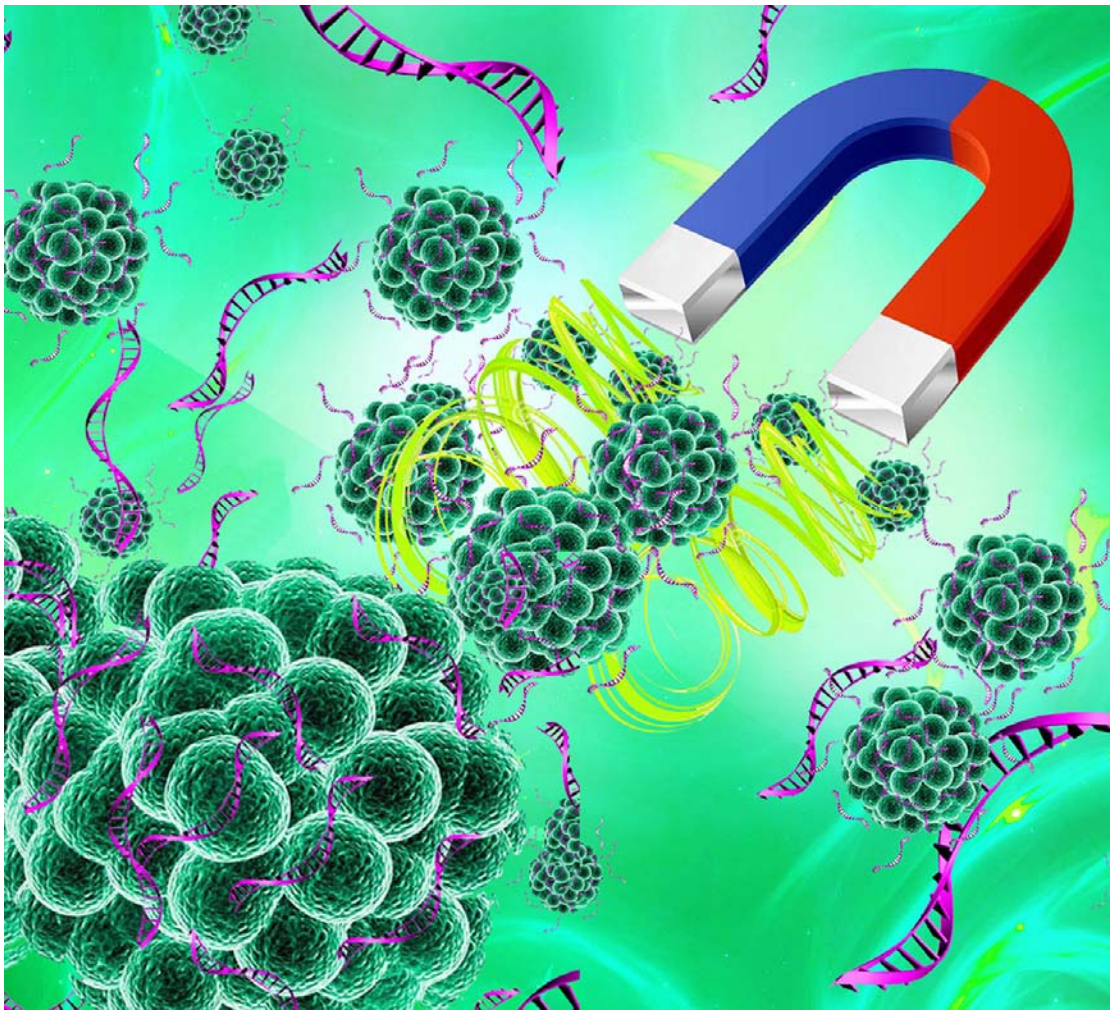

Entry:

Self-Assembled Magnetic Virus-Like Particles for Encapsulation and Delivery of DNA were fabricated using complexes of magnetic surfactants (Mag-Surf) and polyoxometalates (POMs). As an interesting nano-anchor and -motor system, the virus-shaped spheres are colloidal/kinetically stable, relatively highly-ferro-magnetic, positive charge-rich and with high-specific-surface-area. The charge-rich surfaces can attract, capture and migrate bio-molecules like DNA in magnetic field, suggesting a new strategy for biomolecule separations.